Structural Changes in Insulin at a Soft Electrochemical Interface

Hum Bahadur Lamichhane,[1] Terence G. Henares,[1] Mark J. Hackett[1,2,*] and Damien W. M. Arrigan[1,*]

[1]School of Molecular and Life Sciences, [2]Curtin Health Innovation Research Institute, Curtin University, GPO Box U1987, Perth, Western Australia 6845, Australia

** Corresponding authors,*

emails mark.j.hackett@curtin.edu.au (M.J. Hackett), d.arrigan@curtin.edu.au (D.W.M. Arrigan)

ABSTRACT

Understanding the interaction of proteins at interfaces, which occurs at or within cell membranes and lipoprotein vesicles, is central to our understanding of protein function. Therefore new experimental approaches to understand how protein structure is influenced by protein-interface interactions are important. Herein we build on our previous work exploring electrochemistry at the interface between two immiscible electrolyte solutions (ITIES) to investigate changes in protein secondary structure that are modulated by protein-interface interactions. The ITIES provides an experimental framework to drive protein adsorption at an interface, allowing subsequent spectroscopic analysis (e.g., Fourier transform infrared spectroscopy) to monitor changes in protein structure. Here, we reveal that the interaction between insulin and the interface destabilises native insulin secondary structure, promoting formation of alpha-helix secondary structures. These structural alterations result from protein-interface rather than protein-protein interactions at the interface. Although this is an emerging approach, our results provide a foundation highlighting the value of the ITIES as a tool to study protein structure and interactions at interfaces. Such knowledge may be useful to elucidate protein function within biological systems or to aid sensor development.

INTRODUCTION

Insulin, a polypeptide of 51 amino acids, is secreted by pancreatic β cells and, in its monomeric form, regulates glucose metabolism in mammals. Diabetes mellitus in humans is a fatal disease that arises due to deficiency of or inability to use insulin. Globally, in 2015, 415 million people aged between 20 and 79 years suffered from diabetes, 5 million people died due to diabetes, and the global expense of diabetes was USD$673billion.[1] By 2040, the global incidence of diabetes in patients aged between 20 and 79 years is predicted to increase to 642 million people.[1] Since diabetes is caused by variation in insulin concentration and activity, its structure[2–9] and detection[10–17] has been of interest.

The interface between two immiscible electrolytic solutions (ITIES), has been widely used to study the electrochemical behaviour of various proteins,[18–20] particularly as it offers a route to label-free detection.[21] Vanysek and co-workers performed the early studies of proteins such as colicin E_3, bovine serum albumin and ovalbumin at the ITIES and found adsorbed protein at such soft interfaces.[22–24] Subsequent studies revealed the electroactivity of a range of proteins at the ITIES.[12],[10],[25],[19,26],[27] [28] By using alternating current voltammetry, Thomsen et al. studied the adsorption of insulin at the 1,2-dichloroethane-aqueous interface.[13] Likewise, Kivlehan et al. studied the electrochemical nature of bovine insulin at that soft interface,[10] finding that the electrochemical response is due to the formation of a complex between aqueous phase cationic insulin and the hydrophobic anion of the organic phase electrolyte, followed by adsorption of this complex at the interface. Electrochemical adsorption of insulin at the interface was subsequently established by O'Sullivan et al. for the detection of nanomolar concentrations using adsorptive stripping voltammetry.[11] Similarly, Vermehren et al.[7] studied the secondary structures of insulin using Fourier transform infrared (FTIR) spectroscopy within water-organic emulsions and found that the preparation of the emulsion impacted the secondary structures of insulin. However, structural changes in insulin due to its adsorption at the ITIES has not been reported to-date.

A range of techniques like circular dichroism (CD) spectroscopy,[29,30] Raman spectroscopy,[31,32] FTIR spectroscopy,[8,33–35] mass spectrometry,[2] and nuclear magnetic resonance (NMR) spectrometry[6,36] have been used to study the secondary structures of proteins because such structures are important in many diseases.[37] As a result, the secondary structural changes of insulin in various conditions have been studied. Bouchard et al. studied the impact of temperature on the formation of insulin fibrils under acidic conditions using FTIR, CD, and electron microscopy (EM).[3] They found that insulin in solution possessed a substantially α-helical form at pH 2.3 at laboratory temperature, but fibril formation was favorable at 70 ˚C due to the presence of β-sheet secondary structures. Insulin fibril formation on heating was also reported by Nielsen et al.[33] and Nettleton et al.[2] Nault and co-workers characterised insulin behaviour at a hydrophobic surface on a silicon prism functionalized by phenyldimethylmethoxysilane (PDMMS).[38] They observed that when insulin interacted with this hydrophobic surface, it underwent conformational change, from α-helix (at shorter adsorption times) to β-sheet (at longer adsorption times); moreover, the existence of β-sheet resulted in the formation of amyloid fibrils on the hydrophobic surface as also observed by Bouchard et al.[3] at high temperature. Williams[39] analysed the secondary structures of 14 proteins including insulin using Raman spectroscopy, using the amide I Raman band, and compared the results with those of X-ray crystallography. The relative proportions of secondary structures obtained from the Raman method were consistent with the X-ray method. A substantial proportion of combined β-sheet and irregular helix was reported in both cases. Wei et al.[34] also studied the secondary structures of insulin in D_2O using FTIR spectroscopy and compared these results with X-ray crystallography data. They reported that the relative proportions of combined β-sheet and irregular helix was highest among the other secondary structures as found by X-ray crystallography; on the other hand, the content of turn structures was the least abundant. Xie and Tsou[8] compared the secondary structures of insulin and proinsulin using FTIR spectroscopy and found significant proportions of combined β-sheet and irregular helix. Winters et al.[40] reported relative proportions of secondary structures of proteins like insulin, lysozyme, and trypsin in different states i.e. commercial solid, commercial solid in dimethyl sulphoxide (DMSO), and commercial solid in aqueous media. They reported that the different proportions of secondary structures of insulin varied with the solvents used and that significant proportions of insulin β-sheet were present in DMSO compared to in aqueous 0.01 M HCl.

Although many studies of protein secondary structures have been reported, few studies focused on the analysis of the secondary structure of proteins at soft interfaces following electroadsorption. Recently, Booth et al. studied the secondary structures of four proteins, lysozyme, myoglobin, cytochrome c, and Haemoglobin, at the gelled ITIES using FTIR spectroscopy.[5] Following electroadsorption, myoglobin, cytochrome c and Haemoglobin showed unfolding to give antiparallel β-sheets but the structure of electroadsorbed lysozyme was unchanged. They concluded that the secondary structure of proteins is potential independent, but does depend on the interaction between the proteins and organic phase surface. While this summary of the literature shows that there is significant interest in the secondary structures of proteins, the secondary structure of electroadsorbed insulin at the ITIES remains unknown. Despite this, the ITIES combined with spectroscopic analysis offers scope as a platform to study protein interactions with soft interfaces.

The aim of the work reported here was to examine any secondary structural changes of electroadsorbed insulin at the ITIES in a further development of the combination of electrochemistry at the ITIES with FTIR spectroscopy for study of protein structural changes.

EXPERIMENTAL SECTION

Reagents. All reagents were purchased from Sigma-Aldrich Australia and used as received unless indicated. The organic electrolyte salt bis(triphenylphosphoranylidene)ammonium tetrakis(4-chlorophenyl)borate (BTPPATPBCl) was prepared by metathesis of equimolar amounts of bis(triphenylphosphoranylidene)ammonium chloride (BTPPACl) and potassium tetrakis(4-chlorophenyl)borate (KTPBCl).[18] Insulin (bovine pancreas) solutions were prepared freshly each day in 10 mM HCl and refridgerated until used. The organic phase electrolyte solution was 10 mM BTPPATPBCl in 1,2-dichloroethane (DCE) and was gelled by adding low molecular weight polyvinylchloride (PVC) at 10 % at 60 $^{\circ}$C.[41]

Apparatus. Electrochemical measurements were made with an AUTOLAB PGSTAT101 electrochemical workstation (Metrohm, The Netherlands) operated with NOVA software. A Faraday cage was used in all electrochemical experiments. The ITIES used was created within a single hole (diameter 1.56 mm) in a plastic membrane (Melinex S, Polyethylene terephthalate, thickness 0.13 mm). The hole was prepared using a hand punch purchased from a local fabric supply shop; hole diameter and membrane thickness were measured with a USB Digital Microscope (300× magnification, 5 Mpixel image sensor). The geometric area of this single hole was 0.019 cm^2 and hence the ITIES had this assumed geometric area. The single hole plastic membrane was sealed onto the mouth of a glass cylinder using silicone sealant. The gelled organic phase electrolyte was added into the glass cylinder using a slightly heated glass pipette. After one hour, the organic reference solution (aqueous 1 mM BTPPACl and 10 mM LiCl) was placed on top of the organogel in the cylinder. By inserting this assembly in the aqueous phase and adding a pair of Ag/AgCl electrodes, a two-electrode cell was set up. Scheme S1 summarises the electrochemical cell used. Attenuated total reflectance-Fourier transform infrared (ATR-FTIR) spectroscopic measurements were performed on a Thermofisher Scientific Nicolet iS50 FTIR spectrometer (Massachusetts, USA) using a diamond ATR crystal. Spectra were collected with 64 co-added scans and 4 cm^{-1} spectral resolution.

Electrochemical Measurements. A blank cyclic voltammogram (CV) was run on each assembled cell, to confirm absence of impurities and drift on the potential. CVs of tetrapropylammonium ($TPrA^+$) (Figure S1) exhibited diffusion-controlled behaviour, with peak-to-peak separation, ratio of forward and reverse peak currents, and calculated aqueous diffusion coefficient of $TPrA^+$ of *ca.* 60 mV, *ca.* 1 and 5.5 $\times$ 10^{-6} cm^2 s^{-1} (literature value = 8.5 x 10^{-6} cm^2 s^{-1}),[42,43] respectively. CVs of insulin were recorded at varied aqueous concentrations and scan rates; the behaviour was similar to previous results.[10] Subsequently, chronoamperometry (CA) was applied to the interface at different potentials and times in the presence and absence of insulin. The amount of insulin adsorbed at the ITIES was estimated from background-subtracted chronoamperograms.

FTIR measurements. ATR-FTIR spectra of the organogel phase, hydrated films of insulin and solid-state insulin were measured separately by placing the sample directly on the diamond ATR crystal. After CA in the presence or absence of aqueous phase insulin, the organogel was removed from the cell and a thin layer of it placed on the diamond ATR crystal for analysis. Measurements were carried out in triplicate. The amide I peak at the same wavenumber confirmed the reproducibility of the FTIR measurements. A background spectrum of the blank diamond ATR crystal was collected under the same conditions before each sample measurement. Background-subtracted spectra were used for analysis.

The amide I region (1600-1700 cm^{-1})[8] of the spectra were analysed using second derivative and curve fitting techniques.[8,34,44] The second derivatives of the amide I region were taken on 21-point Savitzky-Golay smoothed data. For the curve fitting, the deconvoluted peak positions were assigned to 1693, 1690, 1680, 1660, 1656, 1649, 1637, and 1620 cm^{-1} based on infrared spectra of insulin with known crystallographic data. The peak at 1637 cm^{-1} was assigned to the existence of β-sheet and/or irregular helix (because the vibrational frequencies of β-sheet and irregular helix lie in the same region), and unordered structure, α-helix, and 3_{10}-helix were assigned to 1649, 1656, and 1660 cm^{-1}, respectively. Wavenumbers 1680 and 1690 cm^{-1} were assigned as turn and wavenumbers 1693 and 1620 cm^{-1} were assigned as an

extended chain.[8,33,34] A local least squares method was applied for a 30 second iteration to minimize residuals in the curve fitting.[45] Spectra were analysed using OPUS 7 software.

RESULT AND DISCUSSIONS

Electroadsorption of Insulin. The electrochemistry of proteins at the ITIES has been established to involve cationic protein in the aqueous phase forming a complex with the anion of the organic phase electrolyte and adsorption of this complex at the interface.[5,10,26] Such adsorption of protein at the soft interface opens the path for analysis of protein secondary structures. Here, the electrochemical behaviour of insulin at the interface has been conducted below its isoelectric point (~5.5)[46,47] using an aqueous-organogel system. CV (Figure 1(A)) revealed behaviour in agreement with previous reports, with a reverse peak shape indicative of adsorption.[10–12] Importantly, this potential-induced adsorption enables a chosen fixed potential to be applied to promote adsorption, via CA, from which the surface concentration can be determined.

Protein adsorption at the interface was determined following such electroadsorption from aqueous phases containing either 5, 20, 50, or 100 μM insulin at a fixed adsorption potential (0.70 V) for 30 min. Likewise, using fixed aqueous insulin concentration (20 μM), the protein adsorption for different times was performed. To calculate the amount of adsorbed protein on the interface, the experimentally determined charge passed during the electroadsorption process was substituted in equation (1).

$$Q = z_i F A \Gamma \qquad \text{Eq. (1)}$$

where Q is the background-subtracted charge passed during the electroadsorption, z_i is the molecular charge on insulin (+6 in the acidic conditions used here),[10] F is Faraday's constant (96485 C mol^{-1}), A is the geometric interfacial area (0.019 cm^2), and Γ is the amount of protein adsorbed at the interface (mol cm^{-2}). Experimentally, the amounts of protein adsorbed following electroadsorption of 5, 20, 50, and 100 μM aqueous insulin for 30 min were 1.8, 10.9, 19.6 and 25.8 nmol cm^{-2}, respectively (Figure 1(B)). Since the theoretical close-packed monolayer of insulin was estimated to be 0.0252 nmol cm^{-2},[11] assuming a hydrodynamic radius of 1.35 nm for monomeric insulin,[48] these protein adsorption amounts correspond to multilayers equivalent to ca. 73, 431, 779, and 1025 monolayers at the interface, respectively. This means that with increasing the concentration of insulin in solution, more insulin is adsorbed on the interface. Alternatively, by keeping a fixed insulin concentration (20 μM) and potential (0.70 V), the amount of protein adsorbed can be controlled by the adsorption time. Figure 1(C) shows the amount of protein adsorbed at the interface for different adsorption times. Calculations show that multilayers equivalent to *ca.* 59, 116, 223, and 431 monolayers were formed at the interface at 5, 10, 20 and 30 min adsorption times, respectively. Hence, with the increase in adsorption time, the insulin adsorption at the soft interface can be controlled. In the literature, haemoglobin[18] and lysozyme[49] have also shown multilayer formation at the ITIES. The ability to reproducibly form insulin multilayers on the interface with electrochemical control provides a basis for the FTIR spectroscopic characterisation of these films.

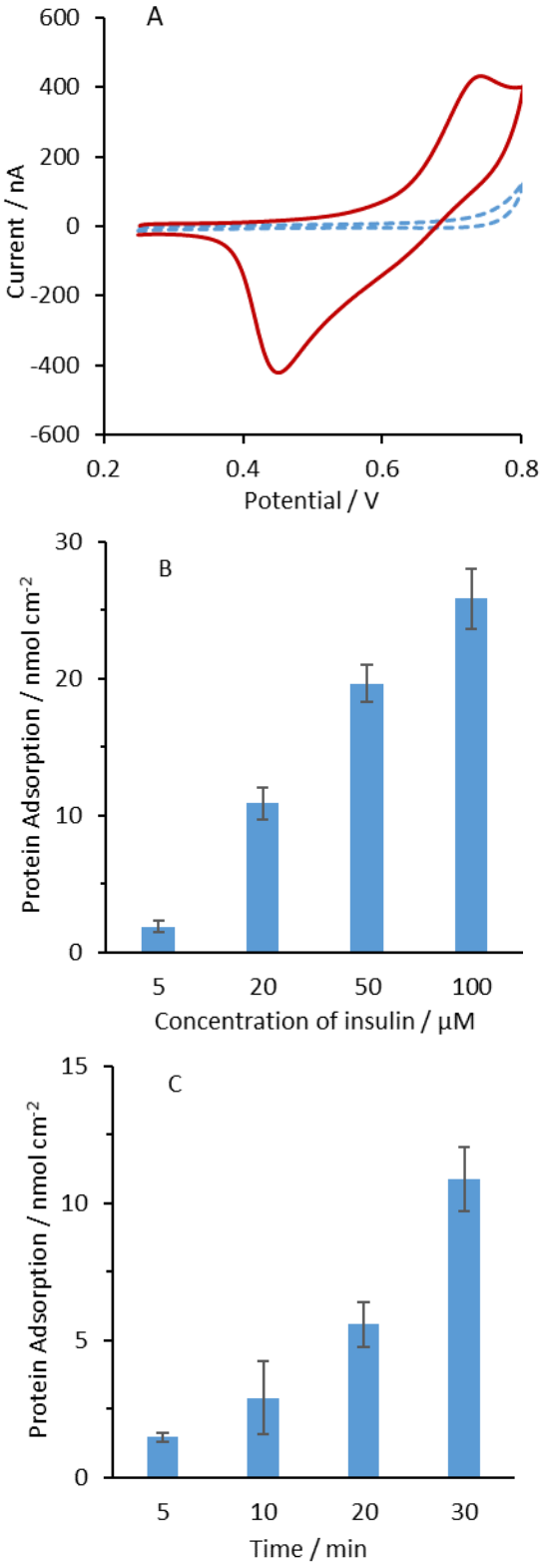

Figure 1. (A) CVs in presence (solid line, 60 µM) and absence (dashed line) of insulin in 10 mM HCl aqueous phase. Organic phase: 10 mM BTPPATPBCl-1,2-DCE (10 % w/v PVC). Scan rate: 10 mV s^{-1}. (B) Protein adsorption at the interface from four concentrations of aqueous phase insulin, 5, 20, 50, and 100 µM. Applied potential: 0.70 V; adsorption time: 30 min. (C) Protein adsorption at the interface for different adsorption times, 5, 10, 20, and 30 min. Insulin concentration: 20 µM; applied potential: 0.70 V. All charges were background subtracted. Error bars are ±1 standard deviation from three experiments.

The effect of applied potential on insulin adsorption. To assess a suitable adsorption potential for FTIR spectroscopy, six different potentials were examined, i.e. 0.35 V, 0.50 V, 0.60 V, 0.65 V, 0.70 V, and 0.75 V. These potentials were chosen to be on either side of the peak potential (Figure 1A). The amide I region of FTIR spectra recorded from the organogel surface following each applied potential experiment are shown in Figure S2(A). The spectra following applications of 0.35 V, 0.50 V, and 0.60 V do not show any distinct amide I absorbance band, indicating that insulin did not adsorb at the interface at these potentials; but the spectra following application of 0.65 V, 0.70 V, or 0.75 V all show distinct amide I features (Figure S2(B)), indicating adsorption of insulin at these potentials (see Figure S3 for data from non-normalised spectra).

It is well known that protein adsorption at the ITIES can be controlled by the potential applied when proteins are in an acidic environment (i.e., pH < pI).[50,51] Here we observed that potential >0.6 V was required to drive insulin adsorption and increased protein adsorption was observed at the interface with increasing applied potential (0.65, 0.70, 0.75 V). However, as shown in Figures S4, S5, and S6, ATR-FTIR did not indicate any change in protein secondary structures associated with electroadsorption at different potentials (20 µM aqueous insulin, 30 min adsorption time). This finding is consistent with previous work reported by Booth et al. for four proteins.[5] Therefore, based on this data, an insulin adsorption potential of 0.70 V was used for all subsequent experiments. Although not the focus of this work, the spectra of electroadsorbed insulin also showed peaks at ca. 800, 1000, and 1100 cm^{-1} that are indicative of insulin-organic anion complex formation (Figure S7).

Confirmation of secondary structures in solid-state and hydrated films of insulin. ATR-FTIR spectroscopy was used to determine the relative proportion of protein secondary structures present in solid-state and hydrated films of insulin. Figures 2(A & B) show the amide I region of the ATR-FTIR spectra and their corresponding second-derivatives, respectively, recorded for solid-state and hydrated films of insulin. The amide I region spectra show a red shift for the hydrated films of insulin relative to the solid-state (Figure 2A), indicating a difference in protein secondary structure. Examination of the second derivative of the amide I region spectra of solid-state and hydrated films of insulin also supports a difference in protein secondary structure (Figure 2B). Specifically, increased second-derivative intensity is observed at 1660 cm^{-1} in the solid state insulin relative to the hydrated film of insulin, while the hydrated film of insulin displays increased second-derivative intensity at 1649 cm^{-1} relative to the solid state. These changes suggest a higher proportion of 3_{10}-helix structures in the solid state, while hydrated films of insulin contain a higher proportion of unordered structure. To confirm the relative proportions of insulin secondary structures , curve fitting of the amide I region (Figure 2C, D) was undertaken and the relative proportions for solid-state insulin and hydrated films of insulin are shown in Figure 2E & F, respectively.

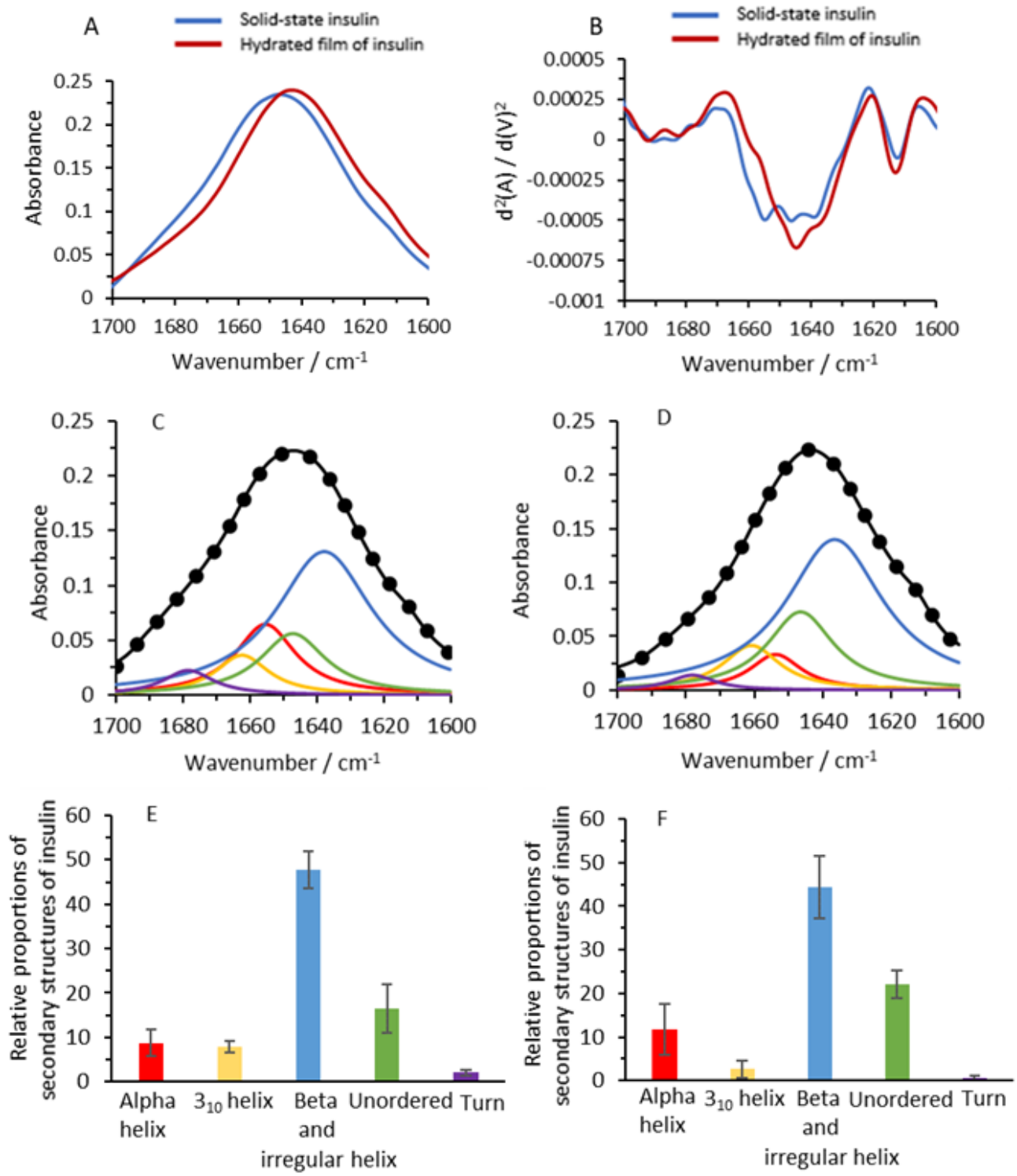

Figure 2. (A) Comparison of amide I regions of solid-state (blue line) and hydrated film of insulin (red line). (B) Comparison of the second derivatives of the amide I region of solid-state (blue line) and hydrated film of insulin (red line). (C) and (D) respectively represent curve fitted FTIR spectra of solid-state and hydrated film of insulin showing the original FTIR band (solid black line), calculated band (black dots) and individual component bands (i.e. α-helix (red line), 3_{10} helix (yellow line), combined β-sheet and irregular helix (blue line), unordered (green line), and turn (violet line)). Plot showing the relative proportions of secondary structures of insulin in (E) solid-state insulin and (F) hydrated film of insulin. Error bars represent ±1 standard deviation obtained from measurements of three independent samples.

The results from curve fitting the amide I region revealed that the dominant secondary structure in both hydrated films of insulin and solid-state insulin is β-sheet and/or irregular helix (we could not differentiate between the two structures in this study, as described in the experimental section). The results for solid-state insulin were consistent with its X-ray crystallography data.[8,34] However, the study revealed that the relative proportions of α-helix in both states of insulin were similar and less than the relative proportions of unordered and β-sheet and/or irregular helix, but higher than turn. In both states, the relative proportions of turns was minor, as reported elsewhere.[8,34] Overall, the shifting of the amide I curve towards lower wavenumber appeared to indicate a conversion of 3_{10}-helix secondary structures to unordered structures.

Dilute aqueous insulin concentration enhances insulin-interface interaction, promoting formation of alpha-helix secondary structures. ATR-FTIR spectroscopy was used to determine if the concentration of insulin in aqueous solution influenced the secondary structure of insulin adsorbed at the interface. Four insulin concentrations, 5, 20, 50, and 100 μM, were used for electroadsorption at the interface (adsorption potential: 0.70 V, adsorption time: 30 min). Figures S8 and S9, respectively, show the amide I band and the second derivative of the amide I band for insulin electroadsorbed from these aqueous concentrations. The spectra show that at more dilute aqueous insulin concentrations, the amide I band was blue shifted toward the higher wavenumber region, indicating a change in secondary structure. Representative curve fitting of the amide I band is shown in Figures 3(A), 3(B), 3(C), and 3(D) for spectra at 5, 20, 50, and 100 μM aqueous insulin concentrations, respectively. The curve fitting indicates that the concentration of aqueous insulin, which controls the amount adsorbed at the interface, influenced the changes to insulin secondary structures. At more dilute aqueous insulin concentration, fewer multilayers are formed, and as a result, there is expected to be a higher ATR-FTIR signal contribution from protein structural changes associated with protein–interface interactions (or protein-protein interactions in close proximity to the interface) relative to protein-protein interactions in layers more distant from the interface. Indeed, ATR-FTIR indicated differences in protein secondary structures as measured for the multilayers adsorbed from different aqueous insulin concentrations (i.e., multilayers of different thickness). Specifically, a higher propensity for the formation of alpha-helices was seen for multilayers produced by adsorption from dilute aqueous insulin solutions, while the multilayers produced by adsorption from greater insulin concentrations showed the presence of combined β-sheet and irregular helix in more substantial proportions. Differences in other secondary structures, like 3_{10}-helix, unordered and turn, were less important, as summarised in Figure 4.

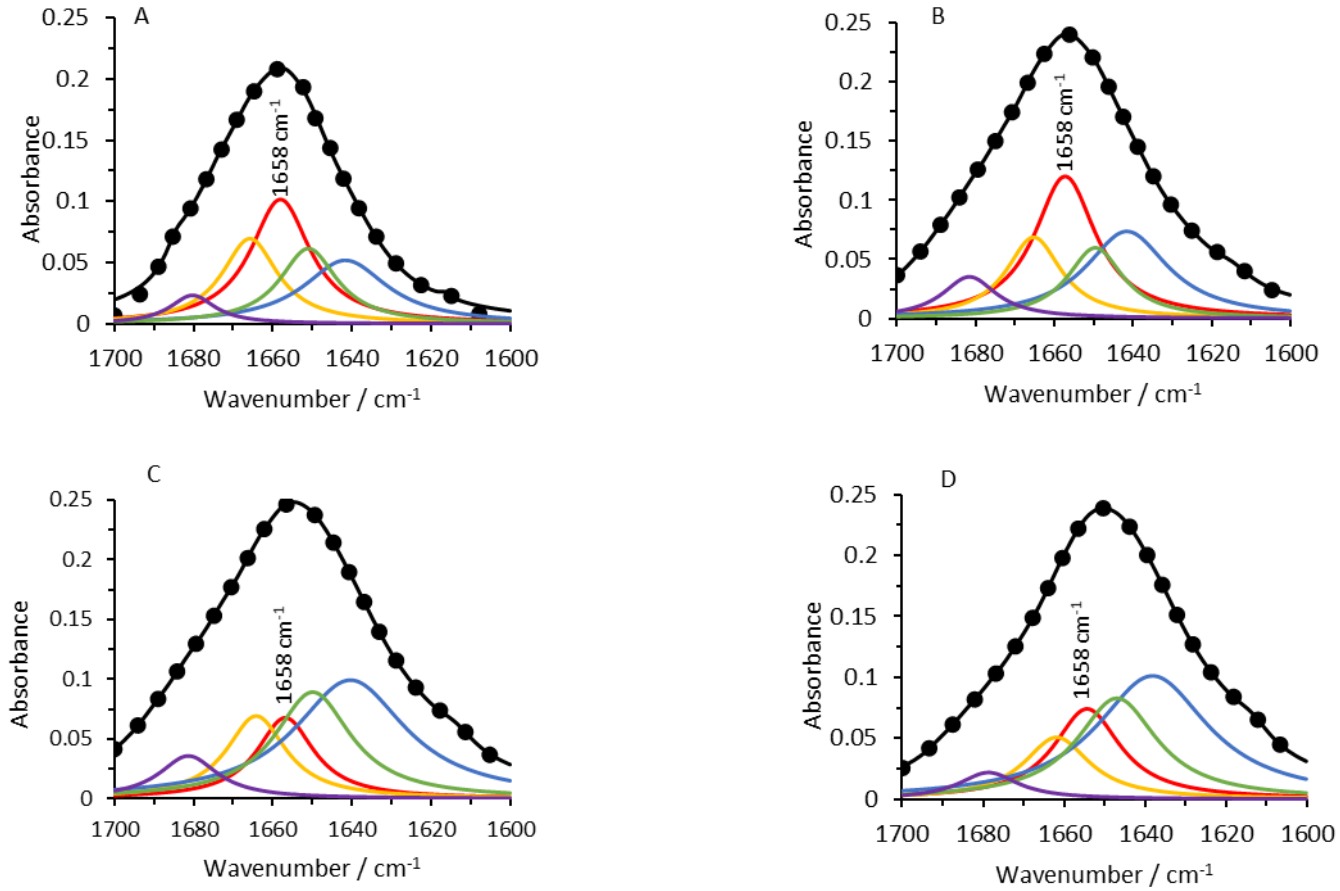

Figure 3. Influence of aqueous phase insulin concentration on the secondary structures detected in electroadosrbed films, showing the original FTIR band (solid black line), the calculated band (black dots), α-helix (red line), combined β-sheet and irregular helix (blue line), 3_{10} helix (yellow line), unordered structures (green line), and turn (violet line). Aqueous phase insulin concentrations: (A) 5, (B) 20, (C) 50, and (D) 100 µM. Adsorption time: 30 min; applied potential: 0.70 V. Aqueous phase 10 mM HCl, organic phase 10 mM BTPPATPBCl in 1,2-DCE (10 % w/v PVC).

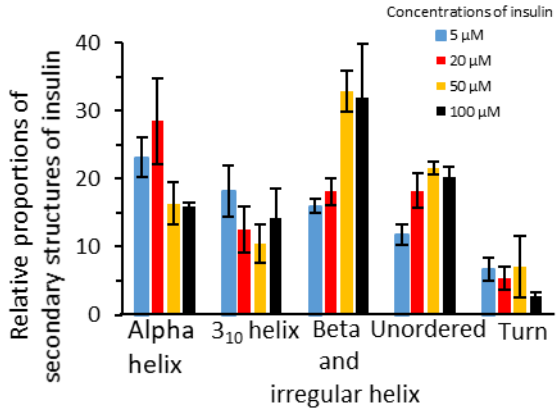

Figure 4. The relative proportions of different secondary structures of electroadsorbed insulin at different aqueous phase concentrations of insulin (5, 20, 50, and 100 µM). Adsorption time: 30 min; applied potential: 0.70 V. Aqueous phase 10 mM HCl, organic phase 10 mM BTPPATPBCl in 1,2-DCE (10 % w/v PVC). Error bars represent ±1 standard deviation obtained from three independent trials.

Figure 5 shows the relationship between the relative intensities of different secondary structures of insulin and the amount of insulin adsorbed on the interface following 30 min adsorption at 0.70 V. Figure 5(A) implies that the lower the amount of insulin adsorbed, the lower is the relative intensity and hence the relative proportion of α-helix present. This is in agreement with the results of Nault et al. for insulin adsorption at the PDMMS-water interface.[38] The relative intensity of combined β-sheet and irregular structure, however, increases with the amount of adsorbed insulin (Figure 5(B)). Figures 5(C), 5(D) and 5(E) show the relationship between relative intensity and the amount of insulin adsorbed for 3_{10} helix, unordered and turn, respectively. It shows that 3_{10} helix, unordered and turn showed less variation with the amount of adsorbed insulin. Overall, a plot of protein secondary structure relative to the amount of adsorbed insulin (Figure 5(F)) highlights the inverse relationship observed for alpha-helix and the combined β-sheet and irregular helix secondary structures. Specifically, alpha-helix secondary structures are more abundant in insulin adsorbed from the more dilute solutions (5 μM and 20 μM) while β-sheet and irregular helix are more abundant in insulin adsorbed from higher concentrations (50 μM and 100 μM).

In this study the electrochemical potential employed during electroadsorption did not influence the secondary structure of the adsorbed insulin, but the concentration of aqueous insulin did, with the most pronounced changes observed for adsorbed multilayers produced from more dilute aqueous insulin solutions. The results suggest that intermolecular interactions between insulin and the aqueous-organic interface drive secondary structural alterations to aqueous insulin to stabilise the formation of alpha helices. As aqueous insulin concentration increases, interactions between insulin and the interface must decrease, while protein-protein interactions between adsorbed insulin will increase. As alpha helixes did not appear to be stabilised in insulin adsorbed from higher aqueous concentration, this study indicates that insulin interactions with the interface, but not protein-protein interactions at the interface, are most likely to stabilise the alpha helix secondary structure. As β-sheet structure is responsible for the formation of insulin amyloids[52] which in turn are responsible for various diseases like systemic amyloidosis, Alzheimer's disease, and maturity onset diabetes,[53] this study could be helpful for the prediction of diseases caused by structural alterations of insulin at interfaces.

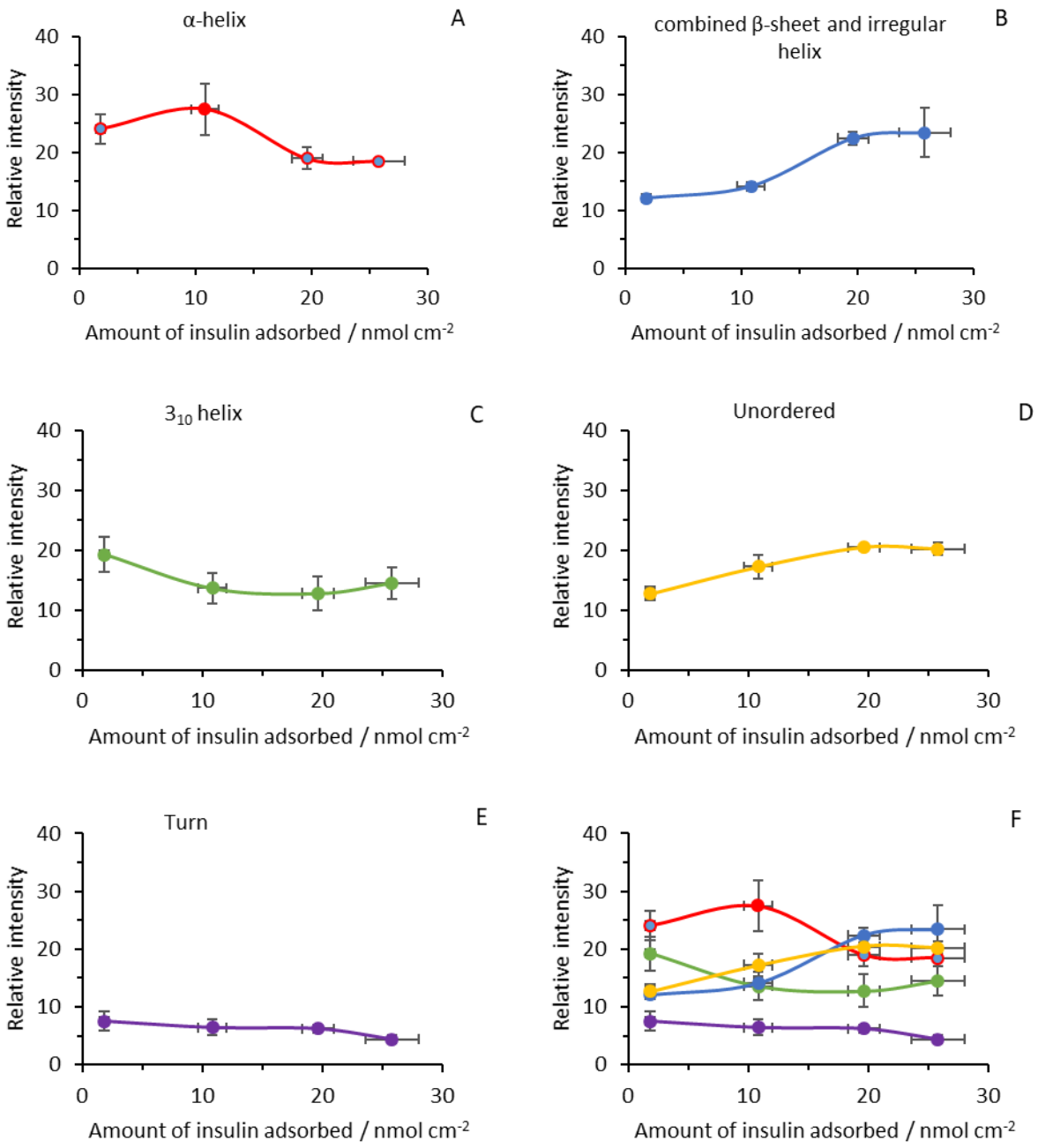

Figure 5. Relationships between relative intensities of different secondary structures of insulin and the amount of insulin adsorbed (A) α-helix , (B) combined β-sheet and irregular helix , (C) 3_{10} helix , (D) unordered , and (E) turn . (F) Comparison of relative intensities of different secondary structures and the amount of insulin adsorbed (i.e. α-helix (red line), combined β-sheet and irregular helix (blue line), 3_{10} helix (green line), unordered (yellow line), and turn (violet line). Adsorption potential 0.70 V, adsorption time 30 min. Error bars represent ±1 standard deviation obtained from measurements of three independent samples.

CONCLUSIONS

Electroadsorption of insulin at the ITIES was studied as a step towards spectroscopic analysis of structural changes. It was found that multilayer films of insulin are formed at the interface. Spectroscopic analysis of solid-state, hydrated film and electroadsorbed insulin was undertaken by ATR-FTIR spectroscopy with emphasis on the Amide I region of the spectra. This allowed the determination of relative proportions of different insulin secondary structures. It was found that the solid-state and hydrated films of insulin possess substantial proportions of combined β-sheet and irregular helix structures. Most importantly, the relative proportions of the secondary structures of electroadsorbed insulin varied with insulin concentrations employed in the electroadsorption step. Lower insulin concentrations were favourable for α-helical structure, while at higher insulin concentrations the combined β-sheet and irregular helix was predominant. However, the 3_{10} helix, unordered and turn secondary structures showed less variation in their proportions with concentration. Likewise, the relative proportions of secondary structures were unaffected by different potentials. In fact, the applied potential was only responsible for the deposition of insulin at the interface. Spectroscopic analysis using the soft interface as a platform is potentially useful to examine secondary structural variations in proteins due to the combination of proteins and hydrophobic species that are found in many biological systems.

Supporting Information.

Additional electrochemical and spectroscopic data. Cell schematic, cyclic voltammograms of tetrapropylammonium ion transfer, amide I region of normalized and non-normalized ATR-FTIR spectra following adsorption, spectra following electroadsorption at different potentials, relative proportions of insulin secondary structures at different potentials, spectra of hydrated film of aqueous insulin, solid state insulin, electroadsorbed insulin, organic phase electrolyte salt and starting material for preparation of organic phase electrolyte salt, spectra of insulin at different concentrations.

REFERENCES

(1) Ogurtsova, K.; Fernandes, J. D. da R.; Huang, Y.; Linnenkamp, U.; Guariguata, L.; Cho, N. H.; Cavan, D.; Shaw, J. E.; Makaroff, L. E. *Diabetes Res. Clin. Pract.* **2017**, *128*, 40–50.

(2) Nettleton, E. J.; Tito, P.; Sunde, M.; Bouchard, M.; Dobson, C. M.; Robinson, C. V. *Biophys. J.* **2000**, *79*, 1053–1065.

(3) Bouchard, M.; Zurdo, J.; Nettleton, E. J.; Dobson, C. M.; Robinson, C. V. *Protein Sci.* **2000**, *9*, 1960–1967.

(4) Yeo, S.-D.; Debenedetti, P. G.; Patro, S. Y.; Przybycien, T. M. *J. Pharm. Sci.* **1994**, *83*, 1651–1656.

(5) Booth, S. G.; Felisilda, B. M. B.; Alvarez de Eulate, E.; Gustafsson, O. J. R.; Arooj, M.; Mancera, R. L.; Dryfe, R. A. W.; Hackett, M. J.; Arrigan, D. W. M. *Langmuir* **2019**, *35*, 5821–5829.

(6) Hua, Q.; Weiss, M. A. *Biochemistry* **1991**, *30*, 5505–5515.

(7) Jørgensen, L.; Vermehren, C.; Bjerregaard, S.; Froekjaer, S. *Int. J. Pharm.* **2003**, *254*, 7–10.

(8) Xie, L.; Tsou, C. L. *J. Protein Chem.* **1993**, *12*, 483–487.

(9) Yu, N.-T.; Jo, B. H.; Chang, R. C. C.; Huber, J. D. *Arch. Biochem. Biophys.* **1974**, *160*, 614–622.

(10) Kivlehan, F.; Lanyon, Y. H.; Arrigan, D. W. M. *Langmuir* **2008**, *24*, 9876–9882.

(11) O'Sullivan, S.; Alvarez de Eulate, E.; Yuen, Y. H.; Helmerhorst, E.; Arrigan, D. W. M. *Analyst* **2013**, *138*, 6192–6196.

(12) Scanlon, M. D.; Strutwolf, J.; Arrigan, D. W. M. *Phys. Chem. Chem. Phys.* **2010**, *12*, 10040–10047.

(13) Thomsen, A. E.; Jensen, H.; Jorgensen, L.; Weert, M.; Østergaard, J. *Colloids Surfaces B Biointerfaces* **2008**, *63*, 243–248.

(14) Zhang, M.; Mullens, C.; Gorski, W. *Anal. Chem.* **2005**, *77*, 6396–6401.

(15) Jaafariasl, M.; Shams, E.; Amini, M. K. *Electrochim. Acta* **2011**, *56*, 4390–4395.

(16) Stankovich, M. T.; Bard, A. J. *J. Electroanal. Chem* **1977**, *85*, 173–183.

(17) Yu, Y.; Guo, M.; Yuan, M.; Liu, W.; Hu, J. *Biosens. Bioelectron.* **2016**, *77*, 215–219.

(18) Alvarez de Eulate, E.; Serls, L.; Arrigan, D. W. M. *Anal. Bioanal. Chem.* **2013**, *405*, 3801–3806.

(19) Alvarez de Eulate, E.; O'Sullivan, S.; Arrigan, D. W. M. *ChemElectroChem* **2017**, *4*, 898–904.

(20) Alvarez de Eulate, E.; Qiao, L.; Scanlon, M. D.; Girault, H. H.; Arrigan, D. W. M. *Chem. Commun.* **2014**, *50*, 11829–11832.

(21) Herzog, G.; Arrigan, D. W. M. *Analyst* **2007**, *132*, 615–632.

(22) Vanýsek, P.; Buck, R. *J. Electrochem. Soc.* **2006**, *131*, 1792–1984.

(23) Vanýsek, P.; Reid, J.; Craven, M.; Buck, R. *J. Electrochem. Soc.* **2006**, *131*, 1788–1791.

(24) Vanýsek, P.; Sun, Z. *Bioelectrochemistry Bioenerg.* **1990**, *23*, 177–194.

(25) Herzog, G.; Kam, V.; Arrigan, D. W. M. *Electrochim. Acta* **2008**, *53*, 7204–7209.

(26) Arrigan, D. W. M.; Hackett, M. J.; Mancera, R. L. *Curr. Opin. Electrochem.* **2018**, *12*, 27–32.

(27) Poltorak, L.; Meijden, N. van der; Oonk, S.; Sudhölter, E. J. R.; Puit, M. de. *Electrochem. commun.* **2018**, *94*, 27–30.

(28) Sakae, H.; Toda, Y.; Yokoyama, T. *Electrochem. commun.* **2018**, *90*, 83–86.

(29) Chen, Y. H.; Yang, J. T.; Martinez, H. M. *Biochemistry* **1972**, *11*, 4120–4131.

(30) Greenfield, N. J. *Nat. Protoc.* **2006**, *1*, 2876–2890.

(31) Tuma, R. *J. Raman Spectrosc.* **2005**, *36*, 307–319.

(32) Lippert, J. L.; Tyminski, D.; Desmeules, P. J. *J. Am. Chem. Soc.* **1976**, *98*, 7075–7080.

(33) Nielsen, L.; Frokjaer, S.; Carpenter, J. F.; Brange, J. *J. Pharm. Sci.* **2001**, *90* (1), 29–37.

(34) Wei, J.; Lin, Y. Z.; Zhou, J. M.; Tsou, C. L. *Biochim. Biophys. Acta* **1991**, *1080*, 29–33.

(35) Tidy, R. J.; Lam, V.; Fimognari, N.; Mamo, J. C.; Hackett, M. J. *Vib. Spectrosc.* **2017**, *91*, 68–76.

(36) Wuthrich, K. *J. Biol. Chem.* **1990**, *265*, 22059–22062.

(37) Carrell, R. W.; Lomas, D. A. *Lancet* **1997**, *350*, 134–138.

(38) Nault, L.; Guo, P.; Jain, B.; Bréchet, Y.; Bruckert, F.; Weidenhaupt, M. *Acta Biomater.* **2013**, *9*, 5070–5079.

(39) Williams, R. W. *J. Mol. Biol.* **1983**, *166*, 581–603.

(40) Winters, M. A.; Knutson, B. L.; Debenedetti, P. G.; Sparks, H. G.; Przybycien, T. M.; Stevenson, C. L.; Prestrelski, S. J. *J. Pharm. Sci.* **1996**, *85*, 586–594.

(41) Scanlon, M. D.; Herzog, G.; Arrigan, D. W. M. *Anal. Chem.* **2008**, *80*, 5743–5749.

(42) Samec, Z. *Pure Appl. Chem.* **2004**, *76*, 2147–2180.

(43) Rahman, M. A.; Doe, H. Ion *J. Electroanal. Chem.* **1997**, *424*, 159–164.

(44) Byler, D. M.; Susi, H. *Biopolymers* **1986**, *25*, 469–487.

(45) Garcia-Quintana, D.; Garriga, P.; Manyosa, J. *Biochim. Biophys. Acta* **1992**, *1122*, 269–272.

(46) Tanford, C.; Epstein, J. *J. Am. Chem. Soc.* **1954**, *76*, 2163–2169.
(47) Gao, J.; Mrksich, M.; Whitesides, G. M.; Gomez, F. A. *Anal. Chem.* **1995**, *67*, 3093–3100.
(48) Oliva, A.; Fariña, J.; Llabrés, M. *J. Chromatogr. B Biomed. Sci. Appl.* **2000**, *749*, 25–34.
(49) Alvarez de Eulate, E.; Arrigan, D. W. M. *Anal. Chem.* **2012**, *84*, 2505–2511.
(50) Scanlon, M. D.; Jennings, E.; Arrigan, D. W. M. *Phys. Chem. Chem. Phys.* **2009**, *11*, 2272–2280.
(51) Arrigan, D. W. M. *Anal. Lett.* **2008**, *41*, 3233–3252.
(52) Jiménez, J. L.; Nettleton, E. J.; Bouchard, M.; Robinson, C. V.; Dobson, C. M.; Saibil, H. R. *Proc. Natl. Acad. Sci. U. S. A.* **2002**, *99*, 9196–9201.
(53) Sunde, M.; Serpell, L. C.; Bartlam, M.; Fraser, P. E.; Pepys, M. B.; Blake, C. C. F. *J. Mol. Biol.* **1997**, *273*, 729–739.

TOC graphic